Polymer 53 (2012) 1393–1403

Contents lists available at SciVerse ScienceDirect

Polymer

journal homepage: www.elsevier.com/locate/polymer

Influence of interdiffusion on multilayered gradient refractive index (GRIN) lens materials

Chuan-Yar Lai*, Michael T. Ponting, Eric Baer

Department of Macromolecular Science and Engineering and Center for Layered Polymeric Systems, Case Western Reserve University, 2100 Adelbert Rd, Cleveland, OH 44106-7202, USA

ARTICLE INFO

Article history:
Received 3 December 2011
Received in revised form
17 January 2012
Accepted 20 January 2012
Available online 28 January 2012

Keywords:
Interdiffusion
Refractive index
Multilayer

ABSTRACT

The interdiffusion of two materials used to fabricate polymeric gradient refractive index (GRIN) lenses was examined by varying contact time during multilayer films co-extrusion composed of alternating poly(methylmethacrylate) (PMMA) and poly(styrene-co-acrylonitrile) with 17 mol% acrylonitrile (SAN17). The model applied successfully described their interdiffusion, and a reasonable mutual diffusion coefficient of 7.0×10^{-13} m^2/s was determined. Atomic force microscopy confirmed good agreement between modeled profiles and actual layer structure, and optical properties were investigated. Films with contact times of $\leq$160 s exhibited multiple refractive indices, while films with longer contact times, showed single refractive indices that followed an additive line. Though a single additive value requires layers $\leq$ a quarter-wavelength of light, these films exhibit such behavior with thicknesses 5$\times$ greater than expected, though layer resolution is still present. Using the model profiles, it was determined that only a 1% reduction in material purity is required to reduce the effective layer thickness.

1. Introduction

Polymeric gradient refractive index (GRIN) materials have the potential to vastly simplify the design of high-quality lens systems. These types of lenses have reduced weight and volumes compared to inorganic lenses, and possess enhanced focusing power and superior aberration correction as compared to traditional monolithic lenses with a single refractive index. GRIN lenses are commonly found in nature, with refractive index differences ranging from as low as 0.03, in the human eye, to 0.22, in a fish eye. Biological GRIN lenses consist of layered assemblies, and their index gradients are obtained through systematic variation in the protein and water concentration [1–8]. A bio-inspired class of synthetic lenses with controlled GRIN distributions was developed previously by assembling polymeric nanolayered films [9,10]. Transparent 4097-layer films of polymethylmethacrylate (PMMA) and poly(styrene-co-acrylonitrile) (SAN17), with individual layer thicknesses below the quarter-wavelength (λ/4) were coextruded at 2% composition steps. Due to the miscibility of PMMA and SAN17 [11,12], mutual diffusion at the layer interfaces occurs during the melt co-extrusion of these films, the amount of interdiffusion dependent on the temperature and the contact time between the two polymers.

During the construction of these GRIN lenses, multiple 4097-layer films of different compositions are stacked and pressed together above the glass transition temperature, during which further interdiffusion between the films can take place. This can affect the final refractive index distribution, and subsequent performance of the lens. Therefore, the understanding of the interdiffusion state of our starting lens materials, the coextruded films, is of utmost importance.

The interdiffusion of PMMA and SAN copolymers has previously been examined in simple bi-layer films using various techniques. Ellipsometry has been used to measure the refractive index profile through thin films of PMMA and SAN (5–40% AN content) annealed at 130 °C. The interfacial thickness determined from the refractive index profile was used to calculate a diffusion coefficient for each polymer pair. The mutual diffusion coefficient of SAN25 (160,000 g/mol) and PMMA (100,000–150,000 g/mol) was between 4×10^{-15} and 7×10^{-15} m^2/s [13]. A different technique, rheometry, has also been utilized to examine PMMA and SAN29 at 120 °C. The dynamic shear viscosity and dynamic complex shear modulus were measured over time, and the composition of the PMMA within the stacked assemblies was determined. The mutual diffusion coefficient was found to be 3.7×10^{-16} m^2/s [14].

Multilayer films have several advantages over other methods for the study of diffusion between polymers. Larger contact areas and a greater number of interfaces between the two materials amplify

* Corresponding author. Tel.: +1 216 368 4162; fax: +1 216 368 6329.
E-mail addresses: chuanyar.lai@case.edu, c.yayalai@gmail.com (C.-Y. Lai).

0032-3861/$ – see front matter © 2012 Elsevier Ltd. All rights reserved.
doi:10.1016/j.polymer.2012.01.036

Table 1
Polymer material characteristics.

Material	Grade	Refractive index (633 nm)	Processing temperature (°C)
Poly(methylmethacrylate)	Plexiglas V920	1.489	255
Poly(styrene-co-acrylonitrile)	Lustran Sparkle	1.573	255

Table 2
Layered sample characteristics.

Number of layers	Total pump rate (rpm)	PMMA/SAN17 Composition (v/v)	Contact time (s)
17	30	90/10, 80/20…20/80, 10/90	105
33	30	50/50	120
65	30	50/50	140
129	10	90/10, 80/20…20/80, 10/90	475
	30	90/10, 80/20…20/80, 10/90	160
257	30	90/10, 80/20…20/80, 10/90	175
513	30	50/50	195
1025	30	100/0, 90/10, 80/20…20/80, 10/90, 0/100	215
Melt blends	30	90/10, 80/20…20/80, 10/90	–

the effect of mutual diffusion. In conjunction with the size scale of these films (50 microns), the effect of interdiffusion can be detected using more common bulk characterization techniques, such as dynamic mechanical thermal analysis, differential scanning calorimetry, and oxygen permeability. Prior interdiffusion studies in multilayers have been carried out, using polymer pairs exhibiting varying degrees of miscibility.

Multilayered films of miscible polycarbonate (PC) and polyethylene terephthalate (PET), with hundreds to thousands of layers, were annealed at various temperatures and times. The glass transitions of the two materials shifted closer together as contact time increased, approaching a single median value when annealed above 200 °C. A model based on Fick's law of diffusion was developed to describe the mutual diffusion at the layer interface, and this model was utilized to determine a reasonable mutual diffusion coefficient that predicted the measured results [15].

Subsequent work examining the interdiffusion of HDPE and LLDPE of high polydispersity using DSC melting peaks required modification of the previous model to fit the experimental data [16,17]. The broad molecular weight distribution caused a very different rate of change in the composition profile, with shorter chains diffusing at faster rates than longer chains. The diffusion coefficient was found to be highly dependent on molecular weight distribution, especially the high molecular weight tail, and less on the dimensions of the phases.

More recently, the previous model for PC/PET was modified to predict the permeability behavior, rather than thermal behavior, of multilayered films composed of nylon and EVOH with differing ethylene contents. The modified model was found to successfully predict the permeability behavior, using reasonable mutual diffusion coefficients consistent with their degree of miscibility [18].

In this work, we advance some results showing the effect of co-extrusion contact time on the interdiffusion state, and the resulting optical properties, of PMMA and SAN17 multilayer films used to build GRIN lenses. The model relating permeability and the interdiffusion state within the layers is applied to predict permeability of the multilayer films, and to determine the mutual diffusion coefficient of PMMA and SAN17. Co-extrusion contact time was varied by increasing the number of layers, as well as varying the pump rates of both polymers.

2. Experimental

Polymethylmethacrylate (PMMA), Plexiglas V920, of $M_w =$ 85,000 g/mol [19], was obtained from Arkema. The poly(styrene-co-acrylonitrile) with 17 mol% acrylonitrile (SAN17), Lustran Sparkle, had a molecular weight of 159,000 g/mol [20]. It was obtained from PolyOne Distribution. Table 1 summarizes the material properties.

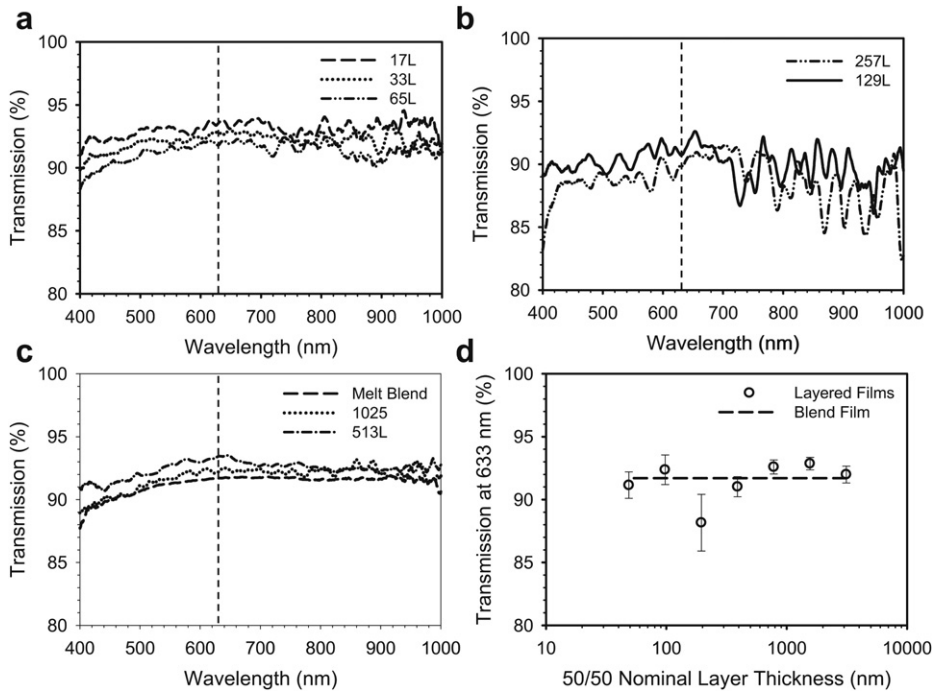

Fig. 1. Transmission of 50/50 PMMA/SAN17 films: a) Representative transmission spectra of 17L, 33L, and 65L films, b) Representative spectra of 129L and 257L films, c) Representative spectra of 513L, 1025L, and blend films, d) Transmission at 633 nm as a function of layer thickness.

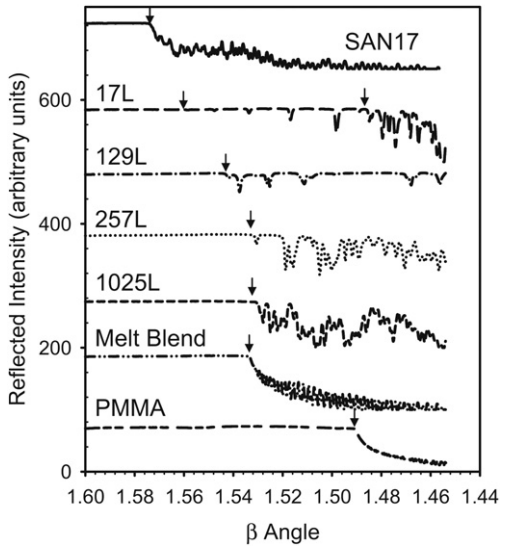

Fig. 2. Raw refractive index curves of 50/50 PMMA/SAN17 and control films.

For this study, films with 17, 129, 257, and 1025 alternating PMMA and SAN17 layers with 100/0, 90/10, 80/20, 70/30, 60/40, 50/50, 40/60, 30/70, 20/80, 10/90, and 0/100 (vol./vol.) compositions were produced through a continuous co-extrusion process using an ATBTA feedblock [21,22], where PMMA was extruded as the A material, and SAN17 as the B, with no third tie (T) material. The polymer melts were extruded through separate single screw extruders, and combined in the ATBTA feedblock. The ABA trilayer (with A layers half the thickness of B) was then sent through a series of multiplication dies, which cut, spread, and stack the melt, doubling the number of layers each time. PMMA was processed at 250 °C and SAN17 was processed at 260 °C. The multipliers were set at 255 °C. Low density polyethylene (LDPE) was used as a protective skin layer, and was peeled off before all testing. A total pump rate of 30 rpm was used to produce films of all layer numbers. Additional 129-layer films were collected at a slower total pump rate of 10 rpm. A single 50/50 composition of 33, 65, and 513 layers was extruded at 30 rpm to better visualize trends in the data. Table 2 lists the films produced, and reports their respective contact/diffusion times, t, calculated from the following equation:

$$t = \left(\frac{\left(nV_{\text{Multiplier}} + V_{\text{Surface}} + V_{\text{Exit}} \right) \text{cm}^3}{(1.2\text{cm}^3/\text{rev})(\text{rev/min})} \right) * (60\ \text{s/min}) \qquad (1)$$

where n is the number of multipliers, V is the volume of each co-extrusion system component, and rev is the pump rate. All overall film thicknesses were kept relatively constant, between 45 and 58 μm, with the target being 50 μm. This thickness variation arises from human error during manual film take-off. Films were stored at room temperature, and LDPE skin layers were removed before all testing.

Refractive index was measured in three different spots along the films with a Metricon Model 2010, which utilizes a prism coupling technique. A free-standing film was held to a prism of known refractive index under pressure, through which a laser light is shone. This setup is then rotated and the refractive index was determined as the drop in reflected laser light intensity detected due to the tunneling of laser light into the film at the critical angle. This critical angle is used by the Metricon to calculate the refractive index of the film, using Snell's Law [23]

$$n_{\text{prism}} \sin\theta_{\text{prism}} = n_{\text{film}} \sin\theta_{\text{film}} \qquad (2)$$

where n is the refractive index and θ is the angle, where n_{prism}, θ_{prism}, and θ_{film} are known.

Transmission measurements of free-standing films ($n = 3$) were collected on an Ocean Optics spectrometer, SD 2000 fiber optic spectrometer and OOI Base 32 software. Transmission within the visible range, at 633 nm to match the laser wavelength of the Metricon prism coupler, was recorded.

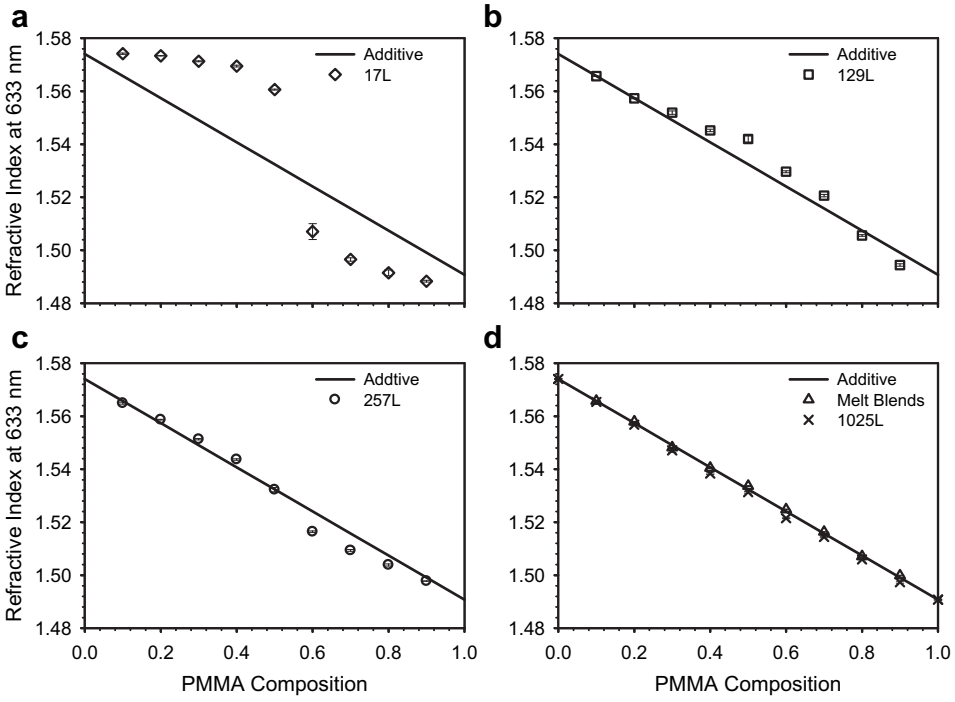

Fig. 3. Change in refractive index with composition at a) 17L, b) 129L, c) 257L, and d) 1025L and melt blends.

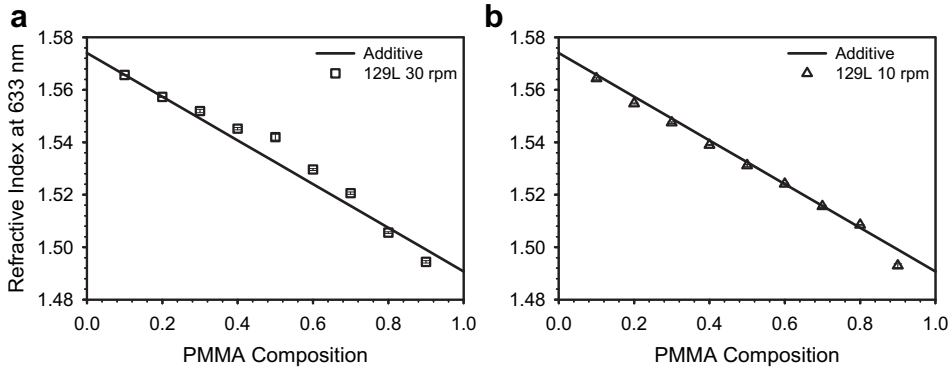

Fig. 4. Change in refractive index of 129L films with composition produced at a) 30 rpm, b) 10 rpm.

Oxygen flux, $J(t)$, at 0% relative humidity, 1 atm, and 23 °C was measured with a MOCON OX-TRAN 2/20. The coextruded films were thick enough to obtain good non-steady state oxygen flux curves, from which permeability P was determined according to [24]

$$P = Jl/p \tag{3}$$

where p is oxygen pressure and l is the film thickness. Two films of each sample were tested to obtain the average permeability.

Films were prepared for atomic force microscopy (AFM) by embedding the films in a 5-min epoxy resin, and cured overnight. Smooth cross-sections were obtained using a cryo-ultramicrotome (MT6000-XL from RMC) at −40 °C, cutting perpendicular to the plane of the film with a glass knife. AFM was then performed in the tapping mode under ambient conditions, using a Nanoscope IIIa MultiMode atomic force microscope from Veeco Instruments with tips of 10 nm diameter. AFM phase images were analyzed using the NanoScope software to obtain a profile showing relative modulus differences across the image.

3. Results and discussion

3.1. Optical properties

The transparency and refractive index of these films can greatly affect the performance of the GRIN lens. High transparency and a single, compositionally dependent, refractive index are required for nanolayered polymer films suitable for the construction of optical quality GRIN lenses. The physical optics of multilayered films of two or more polymers of differing refractive index is quite well known. Wavelength-dependent optical reflections result from the sum of constructive interference of partial reflections at the layer interfaces as light penetrates these materials. The wavelength of the first-order reflection at normal incidence is expressed as [25]

$$\lambda = 2(n_{PMMA}d_{PMMA} + n_{SAN17}d_{SAN17}) \tag{4}$$

Films with layers larger than the wavelength of visible light (>800 nm) will exhibit reflections well away from the visible, and possess distinct separate refractive indices. Films with optical layer thickness (product of refractive index and layer thickness) of a wavelength to a quarter-wavelength thickness (100–800 nm), $\lambda/4$, will reflect in the near-infrared to visible, respectively, with maximum enhancement of reflectance at $\lambda/4$ thickness [26]. When layers are below the $\lambda/4$ thickness, the layers are too thin to give rise to constructive interference, and result in transparent films of a single refractive index.

Fig. 1(a–c) displays representative transmission spectra for 50/50 composition films of different layer numbers. As expected, almost all visible and near-infrared light is transmitted by the thick 3125 nm layers, as these films reflect in the far infrared. As the layer thickness decreased to 1563 and 782 nm, transmission begins to dip in the near-infrared due to higher order reflections. The intermediate layer numbers, with layer thicknesses of 195 and 395 nm, exhibited low intensity first-order reflections in the near-infrared, with several higher order reflections in the visible. The films with thinnest layer thicknesses of 98 and 49 nm also transmit almost all visible and near-infrared light, with spectra very similar to the blend film. As a result, the transmission values in the visible range of the 129- and 257-layer films are slightly lower than those of the 17, 33, 65, and 513, and 1025 layers, Fig. 1d. Even so, transmission remained greater than 85% throughout all compositions, regardless of layer number or pump rate (Figure S.1).

Fig. 2 shows the raw refractive index curves of 50/50 PMMA/SAN17 and control films obtained from a prism coupling technique. Thick 17-layer films exhibited multiple knees and two distinct mode patterns, indicated by arrows. This meant that these layers are still thick enough to exhibit multiple refractive indices. As the number of layers increases, the modes become more mixed, with no distinct patterns, and approach the median refractive index between PMMA and SAN17 controls. For simplicity, the first knee, the highest refractive index within the film, was plotted against composition at each number of layers in Fig. 3(a–d).

Films with 17 layers greatly deviated from the desired additive refractive index, favoring the higher composition material. As contact time increases in 129- and 257-layer films, from 105 to 155

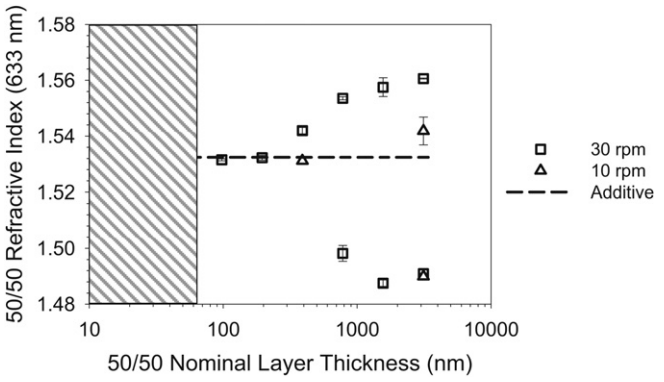

Fig. 5. Change in refractive index of PMMA/SAN17 50/50 composition films as a function of nominal layer thickness. Shaded area indicates layer thicknesses below the quarter-wavelength of visible light.

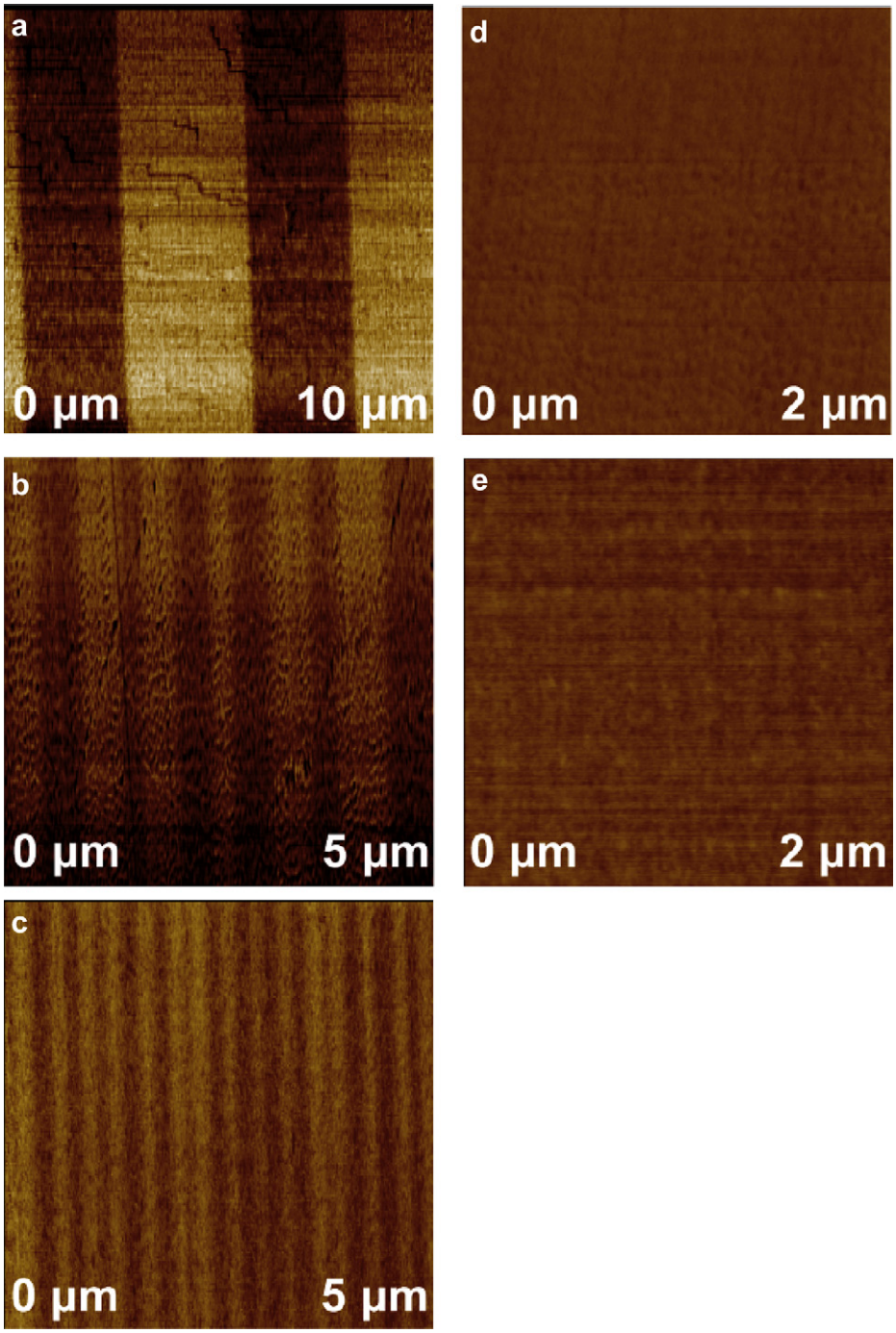

Fig. 6. 50/50 PMMA/SAN17 atomic force microscopy images: a) 17L, b) 129L, c) 257L, d) 1025L, e) melt blend.

and 175 s, respectively, the refractive index approaches that of an additive index, but still does not agree at all compositions. The contact time at these layer numbers is still not long enough for the mutual diffusion of the polymers to reach equilibrium, and sections of pure polymer may still be present. This was more prominent in the middle composition region, since the thinner low composition layers of offset compositions will fully become mixtures at lower contact times than those with more equal layer thicknesses. At 1025 layers, with 215 s of contact time, an additive refractive index is finally achieved at all compositions, behaving much like the melt blends.

Contact time between PMMA and SAN17 was also varied through changes of the pump rate during the co-extrusion process. It can be seen in Fig. 4(a–c) that the refractive index at each composition of these films approaches that of the additive value with decreasing pump rate. Though the nominal layer thickness is much greater than the quarter-wavelength value, $\lambda/4$, interdiffusion has reduced the effective layer thickness to below the quarter-wavelength value, and can exhibit a single refractive index.

This reduction of the effective layer thickness through interdiffusion to give $\lambda/4$ behavior of the refractive index is illustrated in Fig. 5. The change in refractive index of PMMA/SAN17 50/50 composition films as a function of nominal layer thickness is shown to converge nonlinearly from two separate refractive indices to a single refractive index as the layer thickness decreases. The

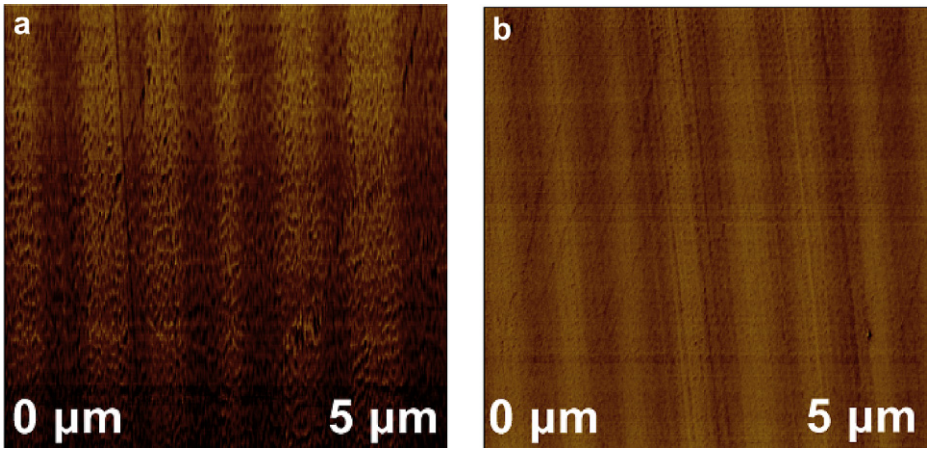

Fig. 7. 50/50 129L PMMA/SAN17 atomic force microscopy images: a) 30 rpm, b) 10 rpm.

shaded area indicates the calculated layer thicknesses below the quarter-wavelength thickness of visible light for a 50/50 composition, using equation (4).

Due to interdiffusion at the interfaces, the refractive indices of 50/50 composition films produced at 30 rpm, with layer thicknesses of 190 nm, are equal to the additive value of layers below the quarter-wavelength. As the pump rate is reduced, increasing contact time from 160 to 475 s, even films with nominal 375 nm layer thickness exhibit below quarter-wavelength behavior. To visualize the effect of interdiffusion on the layered structure, atomic force microscopy (AFM) was performed on cross-sections of the films.

3.2. Atomic force microscopy

Atomic force microscopy images supporting the effect of interdiffusion on the layer structure of 50/50 films is shown in Fig. 6(a–e). PMMA is the dark phase and possesses a lower tensile modulus of ~3.1 GPa, and the light phase is SAN17, with a higher tensile modulus of ~3.2 GPa [27,28]. As expected at 17 layers, the interface between PMMA and SAN17 is sharp and distinct, with little mutual diffusion having occurred. As the layer number increases to 129, and then 257, layers can still be distinguished. However, the interface becomes progressively unclear, and the contrast between the light and dark phases decreases. At 1025 layers, layers are no longer seen, but rather a homogenous blend of the two polymers, which looks very similar to the melt blend. Films with 513 layers also exhibited the appearance of a blend (Figure S.2a). The 129-layer films produced at reduced pump rates exhibited the same trend as those produced with varying layer numbers, Fig. 7(a and b). With increasing contact time, the layer interfaces were seen to become more and more diffuse, while the contrast between light and dark phases decreased.

In order to better understand why the refractive index changes in such a way with increasing contact time, the amount of interdiffusion between the layers must be determined more quantitatively. This was done using oxygen permeability to probe for the interdiffusion between PMMA and SAN17, as PMMA and SAN17 possess dissimilar oxygen permeability values. A model previously developed [18] to relate the permeability of layered nylon and EVOH films and the amount of diffusion at the interfaces was applied to the current system. Composition profiles from the model were then used to give insight into the layer structure.

3.3. Oxygen permeability

Fig. 8 presents the effect of layer number (30 rpm) on oxygen permeability data of the coextruded PMMA/SAN17 films, plotted against a series model and a miscible blend model. SAN17 control films possess a $P(O_2)$ of 0.90 barrer, and PMMA control films have a $P(O_2)$ of 0.07 barrer. These values are reasonable according to literature values for PMMA and SAN polymers [12]. If the layers are discrete, the permeability of the films can be predicted by a series model, described by the following [29]:

$$P_{\text{film}} = \left[\frac{\phi_{\text{PMMA}}}{P_{\text{PMMA}}} + \frac{\phi_{\text{SAN17}}}{P_{\text{SAN17}}}\right]^{-1} \tag{5}$$

P is oxygen permeability and ϕ is the volume composition. If the layers have fully diffused into one another, the permeability of the films can be predicted by a miscible blend model, expressed as [29]

$$\ln P_{\text{film}} = \phi_{\text{PMMA}} \ln P_{\text{PMMA}} + \phi_{\text{SAN17}} \ln P_{\text{SAN17}} \tag{6}$$

At 17 layers, oxygen permeability follows that of a series model, possibly indicating that there is either little interdiffusion between the 2 materials, or the amount of interphase is so small in relation to the layer thickness that it cannot be detected. At the highest number of layers, 1025 layers, the layers are completely diffused together, and the permeability of these films follows the miscible blend model. Films with an intermediate number of layers, 129 and 257, fall between the two models, indicating an intermediate state of interdiffusion between the two polymers.

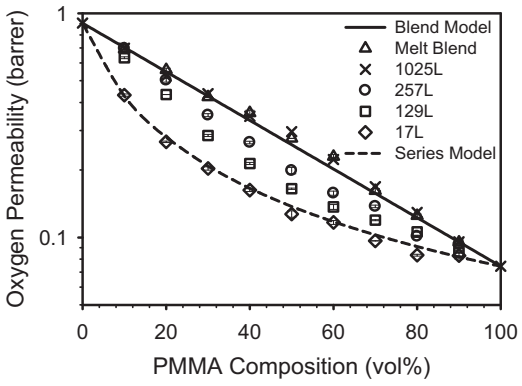

Fig. 8. Oxygen permeability of PMMA/SAN17 films with different layer numbers as a function of PMMA composition.

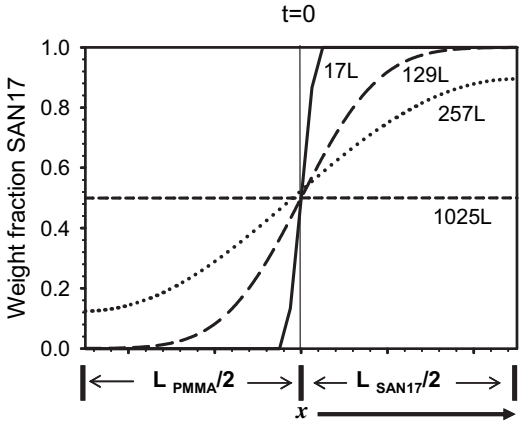

Fig. 9. Weight composition profile of nominal 50/50 composition PMMA/SAN17 films with different contact times.

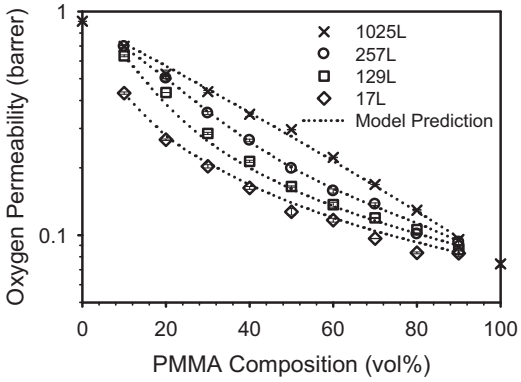

Fig. 11. Model O_2 permeability compared to measured O_2 permeability of PMMA/SAN17 films with different layer numbers as a function of PMMA composition, $D = 7.0 \times 10^{-13}$ m^2/s.

With low contact time during extrusion, the layers remain discrete. As the contact time during extrusion increases, the interdiffusion between the two miscible polymers [13,14] PMMA and SAN17, increases. Eventually, the two polymers become fully diffused into one another, like a blend. A model based on the contact time during the multilayer process and the oxygen permeability can be used to predict the observed permeability trend, and to determine the mutual diffusion coefficient of these two polymers.

of the entire multilayered structure, and the large number of layers allowed end effects to be neglected. The mutual diffusion coefficient, D, was assumed to be constant and independent of composition, and the position of the interface between the diffusing species was assumed to be fixed.

The composition of the layers as a result of interdiffusion can be obtained from Fick's equation for a non-steady state diffusion, accounting for the initial condition of a sharp interface with complete separation of the components, and zero composition gradients at both the boundaries of the interdiffusion element [15]

$$W_{\mathrm{SAN17}}(x,t) = \frac{L_{\mathrm{SAN17}}}{L_{\mathrm{PMMA}}+L_{\mathrm{SAN17}}} + \sum_{m=1}^{\infty}\frac{2}{m\pi}\sin\left(\frac{\pi m L_{\mathrm{SAN17}}}{L_{\mathrm{PMMA}}+L_{\mathrm{SAN17}}}\right)\cos\left(\frac{2\pi m x}{L_{\mathrm{PMMA}}+L_{\mathrm{SAN17}}}\right)\exp\left(\frac{-4\pi^2 m^2 D t}{(L_{\mathrm{PMMA}}+L_{\mathrm{SAN17}})^2}\right) \quad (7)$$

3.4. Modeling the oxygen permeability of the PMMA/SAN17 layered films

A model developed to successfully describe the interdiffusion of nylon and poly(ethylene-co-vinyl alcohol) multilayer film was applied to the present system [18]. To analyze the interdiffusion process, an interdiffusion element was defined as one-half of a PMMA layer together with one-half of the adjacent SAN17 layer and the interface. Only one-half of each layer was required due to the symmetry of the multilayered structure. Uniformity of the layers ensured that the interdiffusion element was representative

$W(x,t)$ is the weight percent composition at position x and diffusion time t, L is the layer thickness.

Fig. 9 shows a weight composition profile of films with nominal 50/50 composition films with varying contact times due to multiplier number. As diffusion will take place within the multiplier dies during the co-extrusion process, layer thicknesses for the model were calculated based on the multiplier dimensions, and not on the final film thickness. Diffusion time, t, was calculated from equation (1), using the number of multipliers, n, the volume of each co-extrusion system component, V, and the pump rate – an arbitrary

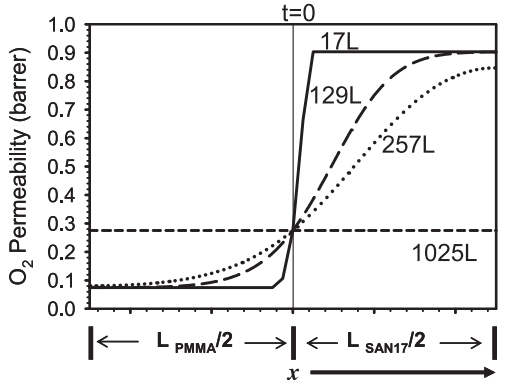

Fig. 10. Permeability composition profile of nominal 50/50 composition PMMA/SAN17 films with different contact times.

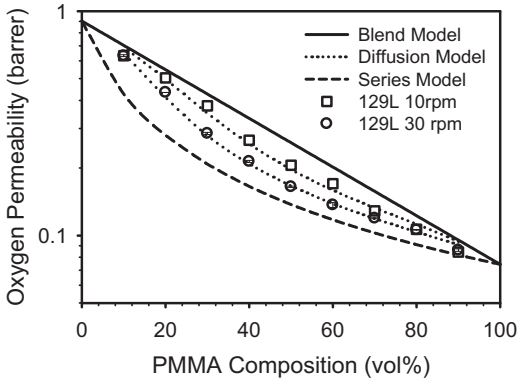

Fig. 12. Oxygen permeability of 129L PMMA/SAN17 films with different pump rates as a function of PMMA composition, compared to the model O_2 permeability, $D = 7.0 \times 10^{-13}$ m^2/s.

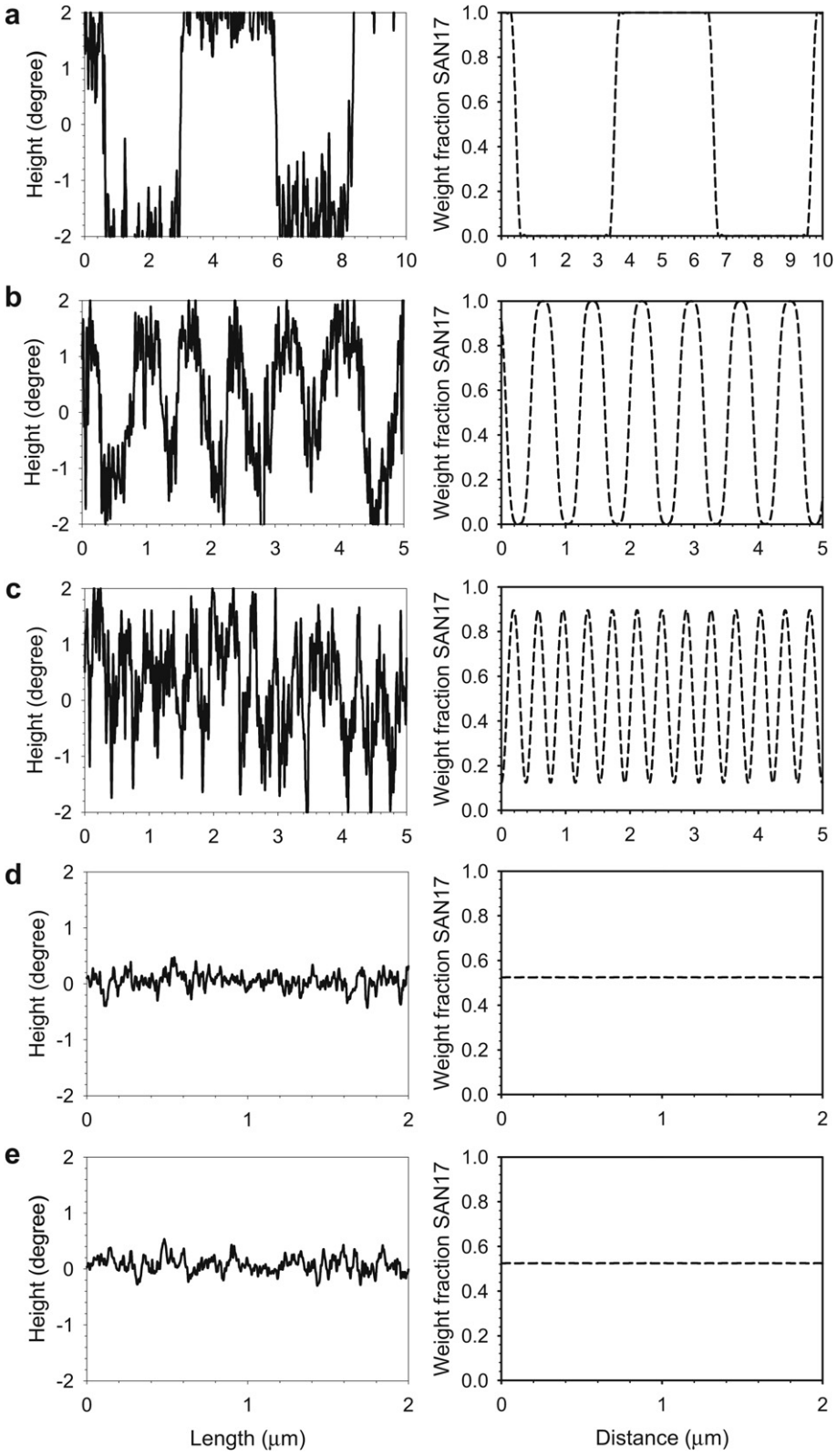

Fig. 13. 50/50 PMMA/SAN17 AFM phase profiles compared to calculated composition profiles, $D = 7.0 \times 10^{-13}$ m^2/s: a) 17L, b) 129L, c) 257L, d) 1025L, e) melt blend.

value at this point. An accuracy of 0.001% was achieved with $m = 15$.

With increasing contact time, the two materials diffuse together at the interface, creating a gradient in the actual composition of the layers. As expected, the composition profile shows the layers progress from almost discrete layers at 17 layers, to a smooth gradient at intermediate layer numbers, and a homogeneous 50/50 blend at 1025 layers. This weight composition profile was then

converted to a permeability profile, using the permeability equation for miscible blends

$$\ln P(x,t) = \phi_{PMMA}(x,t)\ln P_{PMMA} + (1-\phi_{PMMA}(x,t))\ln P_{SAN17} \quad (8)$$

where ϕ_{PMMA} is the volume fraction of PMMA and P_{PMMA} and P_{SAN17} is the permeability of pure PMMA and SAN17, respectively. Fig. 10 shows permeability profiles that were calculated from the corresponding composition profiles in Fig. 9.

Subsequently, the permeability profile was sliced into q equal parts, and the total permeability of the interdiffusion element was calculated from the series model,

$$\frac{1}{P_{calculated}} = \sum_{1}^{q} \frac{1/q}{P(x,t)} \quad (9)$$

An error less than 2% was achieved with $q = 41$. D was varied to match the calculated permeability of the interdiffusion element and the measured film permeability. Given that the measured and calculated permeability from the interdiffusion model for PMMA/SAN17 match well, an accurate determination of the mutual diffusion coefficient, D, can be determined. The best fit data was determined such that the deviation in the model permeability calculation was within the experimental error of the measurement in intermediate layer numbers, 129 and 257. Comparison of the measured film permeability with the calculated permeability obtained using the best fit of D for all the number of layers is shown in Fig. 11. The best fit D found was 7.0×10^{-13} m^2/s, and this value was applied to the 129-layer films produced at lower pump rates.

When contact time was increased through pump rate variation, the permeability increases with decreasing pump rate, which increases the contact time, Fig. 12 displays the oxygen permeability of 129L PMMA/SAN17 films produced at different pump rates as a function of PMMA composition. The permeability is not as high using this method as films with varying layer number at similar contact times, however. This is because increasing the number of layers also increases the number of interfaces where mutual diffusion can occur. The model was again applied, using the previous D value, 7.0×10^{-13} m^2/s, for various layer number films produced at 30 rpm. The model, shown as dotted lines, is also compared to the measured O_2 permeability as a function of PMMA composition in Fig. 12, with very good agreement.

The magnitude of D is reasonable when compared to values of the mutual diffusion coefficient reported for similar miscible polymer pairs. For example, D for PMMA and SAN29 at 120 °C is on the order of 10^{-16} m^2/s [14]. Polymer molecular weights can affect the mutual diffusion coefficient between two materials; interdiffusion increasing with lower molecular weight. In this model, molecular weight was not considered. However, effects of molecular weight on the interdiffusion can be detected through the measured film permeability.

3.5. Relating atomic force microscopy to the model

Fig. 13 shows the calculated composition profiles, using D of 7.0×10^{-13} m^2/s, compared to the AFM phase profiles that represent the difference in moduli across the layers. As PMMA has a lower modulus than SAN17, the phase profile minima represent PMMA-rich material, and maxima represent SAN17-rich material. The composition profiles were very similar in shape to the AFM profiles scanned from AFM images collected. The number of maxima and minima may differ in some samples due to the angle of the AFM images. At 17 layers, the profile shows a very sharp transition between the PMMA and the SAN layers, with plateaus at the minima and maxima equal to each layer thickness. As the number of layers increases to 129 and 257, the transition slope becomes less steep, and the amplitudes decrease. At these layer numbers, there are no plateaus in modulus like before. The layers are thinner in these films, and more mutual diffusion has occurred to create a gradient within the layers. Finally, with 1025 layers, all that is detected is noise, very similar to the profile of the melt blend. A

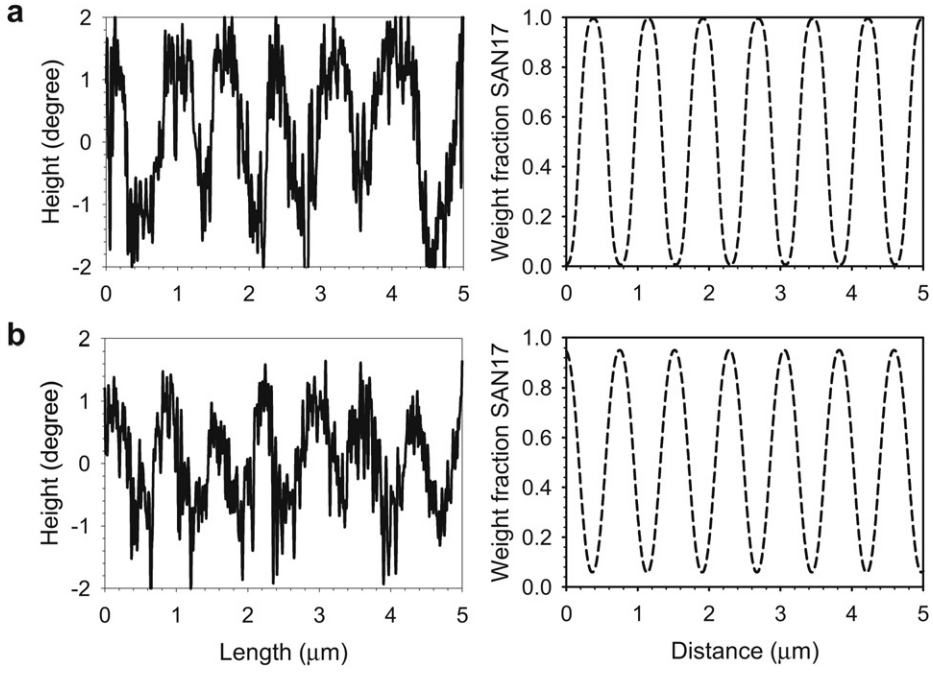

Fig. 14. 50/50 129L PMMA/SAN17 AFM phase profiles compared to calculated composition profiles, $D = 7.0 \times 10^{-13}$ m^2/s: a) 30 rpm, b) 10 rpm.

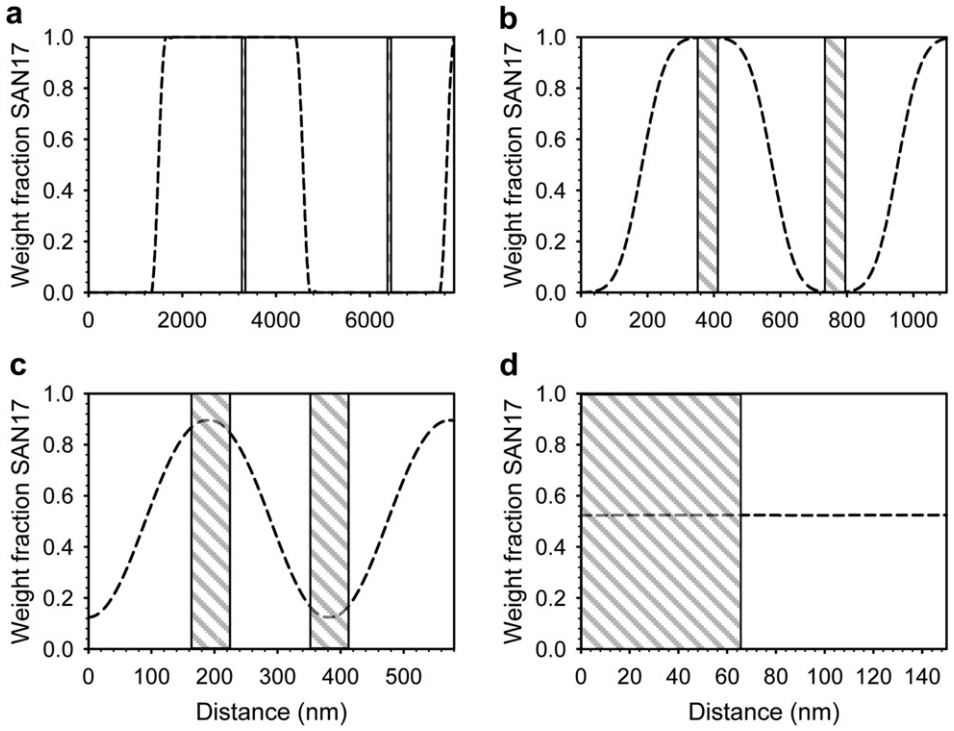

Fig. 15. Composition profiles of 50/50 PMMA/SAN17 (30 rpm) film outer 3 layers used to measure refractive index: a) 17L, b) 129L, c) 257L, d) 1025L. Shaded areas are 65 nm wide, equal to the maximum layer thickness below the quarter-wavelength of a 50/50 composition film.

comparison for the 50/50 513L film is shown in Figure S.2(b-c). Though the AFM phase image appears to be a homogeneous blend, and the signal is noisy, the modulus profile shows that there are still larger amplitude differences than the 1025L films, which was expected.

Variable pump rate 50/50 129L film AFM phase profiles are compared to their calculated composition profiles in Fig. 14(a and b), showing the same trend. The AFM phase profiles showed a gradual change from higher amplitude differences to smaller amplitudes as contact time increased, and the transition between minima and maxima became less and less steep, which match well with the calculated composition profiles. These composition profiles were then used to better understand why layers thicker than the $\lambda/4$ thickness are behaving as layers with thicknesses below the $\lambda/4$, with a single additive refractive index.

3.6. Relating structure to optical properties

As the refractive index is measured using only the outer 3 layers of each film (the outermost being only half that of the others), the outer three layers of the 50/50 calculated composition profiles were then plotted against bars the width of the maximum layer thickness to exhibit a single additive refractive index, Figs. 15 and 16. For 50/50, the maximum layer thickness is 65 nm to give transparent, additive refractive index films. The shaded areas of 65 nm are shown in each composition profile. Layers with less than 65 nm thick sections of greater than or equal to 99% pure PMMA or SAN17, such as those of 17 and 129 layers produced at 30 rpm, resulted in refractive indices that deviate from the additive value. Layers with less than 65 nm thick sections of greater than or equal to 99% pure PMMA or SAN17, however, result in refractive indices that followed the additive line. These films were the ones with 257 or greater

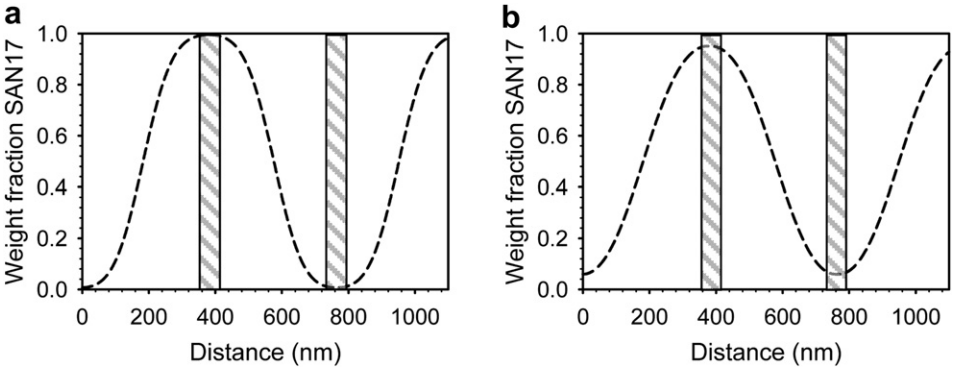

Fig. 16. Composition profiles of 129L 50/50 PMMA/SAN17 outer 3 layers used to measure refractive index: a) 30 rpm, b) 10 rpm.

number of layers, and those with 129 layers produced at lower pump rates.

4. Conclusions

The interdiffusion of two materials used to fabricate polymeric GRIN lenses was followed by studying multilayer films of coextruded alternating PMMA and SAN17, with increasing number of layers and decreasing pump rate. The model applied successfully described the interdiffusion of PMMA and SAN17 produced with these various contact times, and a reasonable mutual diffusion coefficient was determined. AFM confirmed the modeled profiles were in good agreement with actual composition at each number of layers, and optical properties were investigated. Though the optical clarity of these films was not affected by the interdiffusion state due to the miscibility of PMMA and SAN17, the refractive index was greatly influenced. Multiple refractive indices were detected by the prism coupler in films of 17 and 129 layers. 257L, 1025L, and melt blends showed single refractive indices that followed the additive line. Comparison of 50/50 composition films at all layer numbers and pump rates showed that though the maximum layer thickness to produce a single additive refractive index is 65 nm for PMMA and SAN17, nominal layers of 190 nm at 30 rpm pump rate and nominal layers of 375 nm at 20 and 10 rpm rates show an additive refractive index. These samples display such behavior because they have $\leq$65 nm thick sections of $\geq$99% pure material. Interdiffusion essentially decreases the effective layer thickness, and allows for optical behavior equal to layer thicknesses below the quarter-wavelength, although layers are much thicker nominally.

The finding that it only requires a reduction of a material to 99% purity within the calculated maximum quarter-wavelength value to achieve single additive refractive indices within polymer layers is very useful for optics. This effect of interdiffusion can help to optimize the fabrication process of polymeric gradient refractive index lenses. It can also be exploited in future designs of gradient refractive index optics to create novel structures and distributions.

The determined mutual diffusion coefficient of these polymers at temperatures during the lens-making process may be extrapolated from D at the co-extrusion temperature. This will allow for future studies of the interdiffusion at the interfaces between sections of differing compositions in the lens, and give a better understanding of its effect on the resulting lens refractive index distribution and lens performance.

Acknowledgments

This project was made possible through the generous financial support of the National Science Foundation Science and Technology Center, Center for Layered Polymeric Systems (DMR-0423914) and the Defense Advanced Research Projects Agency (DARPA) (HR0011-04-C-0043).

Appendix. Supplementary material

Supplementary data related to this article can be found online at doi:10.1016/j.polymer.2012.01.036.

References

[1] Gullstrand A. In: Southall JPC, editor. Helmholtz's treatise on physiological optics. Washington, DC: Optical Society of America; 1924.
[2] Atchison DA, Smith G. Vision Res 1995;35:2529.
[3] Moffat BA, Atchison DA, Pope JM. Vision Res 2002;42:1683.
[4] Gardneer LF, Smith G, Yao S, Augusteyn RC. Vision Res 2001;41:973.
[5] Berrgman L, Schaefer C. Optics of waves and particles. New York: de Gruyter; 1999.
[6] Jagger WS, Sands PJ. Vision Res 1999;39:2841.
[7] Jagger WS, Sands PJ. Vision Res 1996;36:2623.
[8] Walls GL. The vertebrate eye and its adaptive radiation. New York: Hafner; 1963.
[9] Jin Y, Tai H, Hiltner A, Baer E, Shirk JS. J Appl Polym Sci 2007;103:1834–41.
[10] Beadie G, Shirk JS, Rosenberg A, Lane PA, Fleet E, Kamdar AR, et al. Opt Express 2008;16:11540–7.
[11] Cameron N, Cowie JMG, Ferguson R, Gomez Ribelles JL, Mas Estelles J. Eur Polym J 2002;38:597–605.
[12] Higashida N, Kressler J, Yukioka S, Inoue T. Macromolecules 1992;25:5259–62.
[13] Yukioka S, Nagato K, Inoue T. Polymer 1992;33:1171–6.
[14] Qui H, Bousmina M. Macromolecules 2000;33:6588–94.
[15] Pollock C, Nazarenko S, Hiltner A, Baer E. J Appl Polym Sci 1994;52:163–76.
[16] Schuman T, Stepanov EV, Nazarenko S, Capaccio G, Hiltner A, Baer E. Macromolecules 1998;31:4551–61.
[17] Schuman T, Nazarenko S, Stepanov EV, Maganov SN, Hiltner A, Baer E. Polymer 1999;40:7373–85.
[18] Khariwala D. Structure-property relationships in multilayered polymeric system and olefinic block copolymers. Ph.D. thesis: Case Western Reserve University; 2010.
[19] Saldanha JM, Kyu T. Macromolecules 1987;20:2840–7.
[20] Liu RYF, Bernal-Lara TE, Hiltner A, Baer E. Macromolecules 2005;38:4819–27.
[21] Mueller C, Kerns J, Ebeling T, Narazenko S, Hiltner A, Baer E. Polym Process Eng 1997;97:137–57.
[22] Ponting M, Hiltner A, Baer E. Macromol Symp 2010;294-I:19–32.
[23] Metricon operation manual.
[24] Sekelik J, Stepanov SV, Nazarenko S, Schiraldi D, Hiltner A, Baer E. J Polym Sci Polym Phys 1999;37:847.
[25] Alfrey Jr T, Gurnee EF, Schrenk WJ. Polym Eng Sci 1969;9:400–4.
[26] Pedrotti FL, Pedrotti LS, Pedrotti LM. Introduction to optics. 3rd ed. New Jersey: Pearson Prentice Hall; 2007 [chapter 22].
[27] Arkema Plexiglas V920 literature.
[28] Ineos ABS Lustran SAN Sparkle literature.
[29] Robeson LM. Polymer blends: a comprehensive review. Munich: Carl Hanser Verlag; 2007.